Micromagnetics of Stray Field in Thin-Film Magnetic Materials and Existence of Stable Skyrmions

Nicholas J. Dubicki; *Adjunct Professor, New Jersey Inst. Tech. Newark, NJ*

January 10, 2025

The following is an internal report on progress made by me and my collaborators Cyrill B. Muratov, Anne Bernand-Mantel, Valeriy V. Slastikov, and Theresa Simon of Pisa, IT; Toulouse, FR; Bristol, UK; and Münster, GR respectively. This document serves as a summary of the present methodology in treating the stray field interaction in ferromagnetic films. These models and calculations are treated in finer detail in my dissertation. Here we enumerate the progress made using these models to establish existence criteria for stable magnetic skyrmions. As well, we present several outstanding open questions. The material is to appear in more directed studies in our papers to come.

Contents

1 Summary

The skyrmions are small nanoscopic material defects in a ferromagnetic material, and are of interest to applied physicists, due to their small size and stability properties, for their potential applications to information technology. Their formation is very particular and is the result of multiple competing physical effects within the ferromagnet. In my capacity, I've studied the existence of skyrmions from the point of view of energy minimizing configurations of the micromagnetic energy.

We investigated the role of the material's self-interaction through the magnetic field (called 'stray field' henceforth) in stabilizing magnetic skyrmions in thin multilayered ferromagnetic media. This involved a full characterization of the stray field energy integral in an exact formulation before passing to the asymptotic expansion as the film thickness goes to zero. My analysis revealed a decomposition of the integral into 3 types of interaction, and established an asymptotic hierarchy for the strength of each. In the case of the monolayer, we discovered the exact formulation was able to reveal a regime of skyrmion collapse that was previously unknown. The mode of collapse is a saddle node bifurcation. Meanwhile, the formulation of the multilayer stray field interaction predicts the existence of bound concentric columns of skyrmions, one in each layer.

We are continuing work on refining the numerical simulation of skyrmions in ferromagnetic films to more accurately resolve the aforementioned collapse-existence barrier. We did not anticipate the difficulties we faced with respect to the numerics of stray field interactions of small scale magnetic structure, but this is now becoming an active area of investigation among the micromagnetics community. Future directions of this research could involve using our models for the stray field in multilayered media as perturbative effects in formulations of magnetic skyrmions stabilized by the more commonly studied and applied DMI (Dzyaloshinskii-Moriya Interaction). My preliminary research suggests the stray field perturbation in multilayers with DMI could lead to the formation of new metastable skyrmion configurations. All research so far shows that any potential engineering application of skyrmions is going to require very finely tuned materials, and understanding the competition between each of the magnetic interactions is the first necessary step to properly inform their manufacture. Progression in this direction will go a long way toward the understanding of fundamental physical effects of magnetic materials, and will help to test and justify the use of mesoscopic continuum models at length scales close to atomic.

2 Introduction

Skyrmions are localized solitary regions that can occur in thin magnetic materials and heterostructures. The skyrmion is a defect which resembles a nanoscopic circular domain that achieves the opposite magnetization of its surroundings at a single point. A fundamental stepping stone, Belavin and Polyakov first showed the existence of topologically nontrivial magnetic structure in 2D materials [2]. The magnetic skyrmion would not become a theoretically well-formed concept until 1989 when Bogdanov, Kudinov, and Yablonskii were able to characterize stable isolated "vortex" states in films under the influence of interfacial interactions [12, 11]. They have since been observed in laboratory experiments, first in 2009 [38], (for further developments in experiments, see review papers: [13, 35, 47, 50]).

The study of magnetic materials at the nanoscale is indispensable in the age of computers. The magnetic skyrmions are of some interest to this end due to the fact that they appear as stable material defects in an otherwise uniformly magnetized sample. A skyrmion can be nucleated, deleted, and made to translate like a soliton by passage of electric currents in their vicinity, making them candidates for information carriers [21, 43, 46, 51]. Such proposals, however, rely on accurate understanding of the skyrmions' stability properties, as they are known to degrade under thermal noise [9, 10, 25, 33, 42]. Several authors have worked to give criterea for room temperature stability of skyrmions [3, 16]. This sensitivity also makes the skyrmion a model test case from which material scientists can evaluate and manufacture diverse alloys and heterostructures, as well as more exotic magnetic materials such as ferrimagnetics and antiferromagnetics [1, 17, 27, 34].

There is a long line of study of continuum models for magnetic materials going back to Landau and Lifshitz referred to as the Micromagnetic Theory [31, 30]. We make our deposition in explaining the role of the stray magnetic field in skyrmion stabilization in multilayered materials. This builds on past work on the theory to properly incorporate the stray field in the potential theoretic sense. The leading order stray field interaction in a thin layer was only found as recent as 1997 by Gioia and James [24]. Later

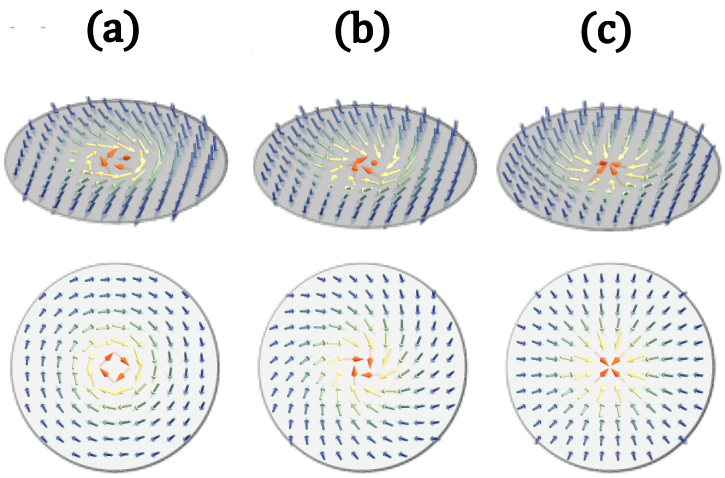

Figure 1: Schematic diagrams of magnetic skyrmions in the plane. (a) Bloch skyrmion, (b) Hybrid skyrmion, (c) Néel skyrmion.

research began to show the higher order, nonlocal effects of stray field could enable skyrmion formation [16], even before their corresponding asymptotic expansion was obtained by Knüpfer, Muratov, and Nolte in 2019 [28, 39]. We have since extended and generalized these results to the multilayer system [18, 5], and critically evaluated the predictive capabilities of the asymptotic regime compared to a finite-thickness representation [4]. This analysis has practical relevance to producing and studying skyrmions in ferrimagnetic systems, as the inherent reduced stray field interaction allows the competition between exchange and stray field interactions to occur over broader length scales than that of ferromagnets, ensuring the resultant structures have length scales greater than that of atomic spacing and thus amenable to the continuum models. Such parameter regimes were studied for a monolayer under applied field, stray field, and DMI by Bernand-Mantel et al. to find stable skyrmions in the low DMI regime [7, 6].

3 Methods

3.1 The Micromagnetic Model

Micromagnetics is a continuum modeling framework that describes the local magnetic moments in a ferromagnet as a three-dimensional vector field $\mathbf{M}$ which has a fixed length and whose properties are governed by an energy functional $E(\mathbf{M})$. It was introduced in 1935 by Landau and Lifshitz to describe the formation of magnetic domains [30]. The search for stable configurations involves variational analysis and the minimization of $E(\mathbf{M})$. A mature summary of the theory can be found in the 1963 monograph by W. F. Brown [14]. For the role of the theory applied to experimental technique, see the book by Hubert and Schäfer [26].

The vector field, $\mathbf{M} : \Omega \to \mathbb{R}^3$, is the magnetization density of a ferromagnetic material occupying a set Ω, and is defined to be zero on Ω^c. The magnitude $M_s = |\mathbf{M}|$ is referred to as the "saturation magnetization" and is assumed to be constant inside Ω. When the magnetization is not stable or metastable the magnetic configuration evolves with time to reduce the energy, unless additional external influences are present. The evolution of the material magnetization is governed by the Landau-Lifshitz-Gilbert Equations (LLG) [26, 31],

$$\left(1+\alpha^2\right)\frac{\partial \mathbf{M}}{\partial t} = -\gamma_0\left(\mathbf{M}\times\mathbf{H}_{\text{eff}} + \frac{\alpha}{M_s}\,\mathbf{M}\times\left(\mathbf{M}\times\mathbf{H}_{\text{eff}}\right)\right); \quad \mathbf{H}_{\text{eff}} = -\frac{1}{\mu_0}\frac{\delta E}{\delta \mathbf{M}}, \tag{1}$$

the evolution depends directly on the so called effective field $\mathbf{H}_{\text{eff}}$, and $\delta E/\delta \mathbf{M}$ represents the functional derivative of the energy with respect to the magnetization. At a stationary point of the energy, the field vanishes and this is simultaneously a fixed point of the LLG equations. The three constants are

γ_0, the gyromagnetic ratio and α, the LLG damping parameter and μ_0, the magnetic permeability of a vacuum.

The energy is expressed as a sum of the different magnetic interactions,

$$\begin{aligned}\mathcal{E}(\mathbf{M}) = &\frac{A}{M_s^2}\int_\Omega |\nabla \mathbf{M}|^2 d^3r + K\int_\Omega \Phi_{an}\left(\frac{\mathbf{M}}{M_s}\right) d^3r + \frac{D}{M_s^2}\int_\Omega F_{DMI}(\mathbf{M}, \nabla\mathbf{M}) d^3r \\ &- \mu_0 \int_\Omega \mathbf{M}\cdot\mathbf{H}_a \; d^3r + \frac{\mu_0}{2}\int_{\mathbb{R}^3} |\mathbf{H}_d(\mathbf{M})|^2 d^3r.\end{aligned} \tag{2}$$

Each term represents one type of interaction, with functional dependence on the magnetization, $\mathbf{M}$. In order of appearance they are the exchange, E_{ex}; the crystalline anisotropy, E_{an}; the Dzyaloshinskii-Moriya Interaction, E_{DMI} (also called antisymmetric-exchange); the interaction with applied field, E_Z (this energy is called the Zeeman energy); and the stray field energy, E_d (or demagnetizing energy).

Exchange is characterized by the stiffness, A, and measures nonuniformity of the magnetic texture, so promotes uniformity when minimized [30]. The anisotropy, E_{an}, is characterized by the constant, K, measures deviation from preferred directions of magnetization, according to the material's crystal structure. The function Φ_{an} should be invariant with reversal of the direction of $\mathbf{M}$. In the case of uniaxial anisotropy, $\Phi_{an}(\mathbf{m}) = m_1^2 + m_2^2$, which is zero and minimal when $\mathbf{m}$ is aligned with the third axis [31]. The Dzyaloshinskii-Moriya Interaction (DMI) is characterized by the constant, D, and induces a spacial twisting effect [19, 37]. The function F_{DMI} is some bilinear form depending on $\mathbf{M}$ and its derivatives that changes sign with reversal of the direction of $\mathbf{M}$. The Zeeman energy is that stored in the interaction between the material magnetization and an applied field, $\mathbf{H}_a$. This interaction is minimal when the material magnetization aligns with the applied field. The stray field is the magnetic field, $\mathbf{H}_d$, which is generated by the spins themselves, hence the dependence $\mathbf{H}_d(\mathbf{M})$. This interaction tends to counteract the uniformity promoting mechanisms of exchange and anisotropy, leading to the formation of magnetic domains [26, 30], and skyrmions [3, 4, 18].

The stray field comes from the solution of the stationary Maxwell's Equations in the form of a magnetic scalar potential, $\mathbf{H}_d = -\nabla U_d$, where U_d is ultimately a fundamental solution of Poisson's Equation,

$$U_d = -\frac{1}{4\pi}\int_{\mathbb{R}^3} \frac{\nabla\cdot\mathbf{M}(\mathbf{r}')}{|\mathbf{r}-\mathbf{r}'|} d^3r', \tag{3}$$

which has to be understood in the distributional sense, as the free surface, $\partial\Omega$, begets delta-function singularities in $\nabla\cdot\mathbf{M}$ [22]. In our results, the stray field energy plays a prominent role, and we will see how to treat it in the thin-film layer geometry in subsequent sections.

3.2 The Micromagnetic Model for Ferromagnetic Layers

In a system of ferromagnetic layers, each of thickness d, one scales the energy as $E = \frac{\mathcal{E}}{Ad}$. The magnetization vector can be decomposed as $M_s\mathbf{m} = \mathbf{M}$, such that $|\mathbf{m}| = 1$. Now, we may define the characteristic exchange length, l_{ex} and introduce the following relevant dimensionless quantities which appear in the final result:

$$l_{ex} = \sqrt{\frac{2A}{\mu_0 M_s^2}}\,, \qquad Q = \frac{2K}{\mu_0 M_s^2}\,, \qquad \kappa = D\sqrt{\frac{2}{\mu_0 M_s^2 A}}\,, \qquad \delta = \frac{d}{l_{ex}}. \tag{4}$$

The multilayer model is characterized by having multiple magnetization fields, $\mathbf{m}_i : \mathbb{R}^2 \to \mathbb{S}^2$, one for each layer. This assumes negligible variation in $\mathbf{m}_i$ in the vertical direction. The principal subscript will always be used to identify the field $\mathbf{m}_i$. When components need to be referenced, a secondary subscript will be introduced, $\mathbf{m}_i = (\mathbf{m}_{i,\perp}, m_{i,\parallel})$. Where the subscripts -$\perp$ and -$\parallel$ refer to the in-plane component and the out of plane component of $\mathbf{m}_i$ respectively, see Figure 2.

There are N layers of non-dimensional thickness, δ, separated by nonmagnetic layers of thickness $(a-1)\delta$, as diagrammed in Figure 2. As such, the thickness of the entire system will be $\mathcal{O}(N\delta)$. The magnetization may be represented as the combination of the magnetizations of each layer,

$$\mathbf{m}(x,y,z) = \sum_{i=1}^{N} \chi_{\omega_i}(z)\mathbf{m}_i(x,y). \tag{5}$$

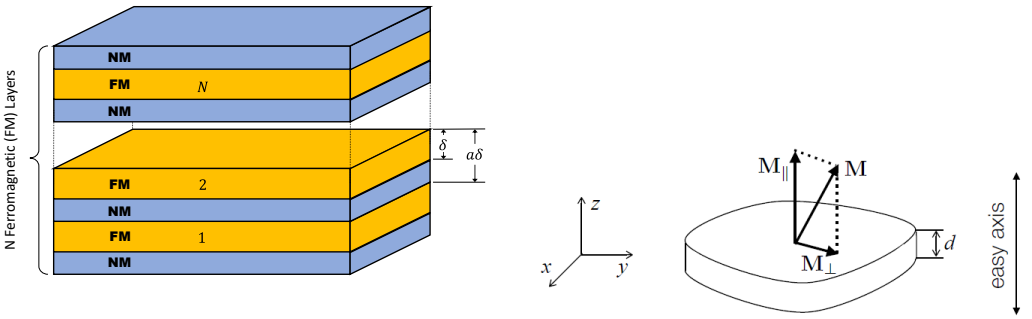

Figure 2: Left: Schematic of a characteristic N-layer ferromagnetic (FM) system with identical layers of thickness δ. Each ferromagnetic layer is separated by $(a-1)\delta$ by non-magnetic (NM) spacer layers. Right: Schematic film showing decomposition of $\mathbf{M}$ into in-plane and out-of-plane components.

where χ_{ω_i} are the characteristic functions of each layer, and $\omega_i = [a\delta(i-1), \delta + a\delta(i-1)]$.

We assume the ferromagnetic layers are the same material, and therefore have the same exchange stiffness, interfacial DMI strength, and uniaxial out-of-plane anisotropy. This will give particular choices for the forms of E_{an} and E_{DMI} presented in generality before,

$$E_{an} = Q \sum_{i=1}^{N} \int_{\Omega} |\mathbf{m}_{i,\perp}|^2 d^2 r, \tag{6}$$

$$E_{DMI} = \sum_{i=1}^{N} \kappa_i \int_{\mathbb{R}^2} \left(m_{i,\parallel} \nabla \cdot \mathbf{m}_{i,\perp} - \mathbf{m}_{i,\perp} \cdot \nabla m_{i,\parallel} \right) d^2 r \tag{7}$$

where integration has already been carried out in the vertical coordinate. We do allow separate layers to differ in the sign of κ_i. Each layer has its own fundamental self-interaction energies, resulting in a summation, and an additional $N-1$ interlayer exchange coupling interactions between a layer and its neighbors. The energy, measured in the units Ad is

$$\begin{aligned} E\left(\{\mathbf{m}_i\}\right) = &\sum_{i=1}^{N} \int_{\mathbb{R}^2} \left(|\nabla \mathbf{m}_i|^2 + Q \left|\mathbf{m}_{i,\perp}\right|^2 + \kappa_i \left(m_{i,\parallel} \nabla \cdot \mathbf{m}_{i,\perp} - \mathbf{m}_{i,\perp} \cdot \nabla m_{i,\parallel} \right) \right) d^2 r \\ &+ E_d\left(\{\mathbf{m}_i\}, \delta\right) + \sigma \sum_{i=1}^{N-1} \int_{\mathbb{R}^2} \left|\mathbf{m}_{i+1} - \mathbf{m}_i\right|^2 d^2 r, \end{aligned} \tag{8}$$

where the last term is the interlayer exchange coupling with the constant σ. The stray field energy, E_d, gives additional self-interactions and interlayer coupling terms and shall be treated in the subsequent sections. The stray-field energy is

$$E_d(\{\mathbf{m}_i\}, \delta) = \frac{1}{\delta} \int_{\mathbb{R}^3} \left(|\mathbf{h}_d|^2 - \sum_i \chi_{\omega_i}(z) \right) d^3 r, \tag{9}$$

where in this definition, a constant has been subtracted from the field energy density within Ω to result in a bounded integral.

3.3 Scheme of Stray-Field Integral Kernels

Due to its complexity and nonlocal nature, various treatments of (9) are available, in particular, one desires to pass to the asymptotic limit as $\delta \to 0$. The first step is to isolate the contributions from each $\mathbf{m}_i$ vector field, by Fourier transforming in the vertical coordinate. This breaks the integral, (9) into

a matrix of different nonlocal interaction terms, each featured as a quadratic form with some kernel. This representation was a fundamental result of my thesis that was necessary to better characterize skyrmions as acted upon by the stray field in multilayers [18].

The magnetization appropriately decomposed into its in-plane and out-of-plane components in the layered system is

$$\mathbf{m}(\mathbf{r}, z) = \sum_{i=1}^{N} \tau_z^{a\delta(i-1)} \chi_{[0,\delta]}(z) \left(\mathbf{m}_{i,\perp}(\mathbf{r}) + \hat{\mathbf{e}}_3 m_{i,\parallel}(\mathbf{r}) \right), \tag{10}$$

where τ_z is a translation operator acting on χ. We assume for all i, $\mathbf{m}_{i,\parallel} \to \pm\hat{\mathbf{e}}_3$, as $\mathbf{r} \to \infty$. The calculation is too detailed to include here, but in spirit, plugging the above into (3) and applied to (9) will yield, after careful manipulation [18],

$$E_d(\{\mathbf{m}_i\}, \delta) = \sum_{p=1}^{N} \left\{ - ||\mathbf{m}_{p,\perp}||^2_{L^2(\mathbb{R}^2)} + \sum_{q=1}^{N} \left(E_{vol}^{(pq)} + E_{vs}^{(pq)} + E_{surf}^{(pq)} \right) \right\}. \tag{11}$$

By virtue of the negative sign of the first term, the stray field interaction desires the magnetization to lie in plane. Thus $Q > 1$ is required and assumed. The component energies are

$$E_{vol}^{(pq)} = \frac{1}{\delta} \int_{\mathbb{R}^2} \int_{\mathbb{R}^2} K_{vv}^u(|\mathbf{r} - \mathbf{s}|)(\nabla \cdot \mathbf{m}_p^\perp(\mathbf{r}))(\nabla \cdot \mathbf{m}_q^\perp(\mathbf{s}))\ d^2r\ d^2s, \tag{12}$$

$$\begin{aligned} E_{vs}^{(pq)} = &\frac{1}{\delta} \int_{\mathbb{R}^2} \int_{\mathbb{R}^2} K_{vs}^u(|\mathbf{r} - \mathbf{s}|)(\nabla \cdot \mathbf{m}_p^\perp(\mathbf{r}))(m_q^\parallel(\mathbf{s}) + 1)\ d^2r\ d^2s \\ &- \frac{1}{\delta} \int_{\mathbb{R}^2} \int_{\mathbb{R}^2} K_{vs}^u(|\mathbf{r} - \mathbf{s}|)(m_p^\parallel(\mathbf{r}) + 1)(\nabla \cdot \mathbf{m}_q^\perp(\mathbf{s}))\ d^2r\ d^2s, \end{aligned} \tag{13}$$

$$E_{surf}^{(pq)} = -\frac{1}{2\delta} \int_{\mathbb{R}^2} \int_{\mathbb{R}^2} K_{ss}^u(|\mathbf{r} - \mathbf{s}|) \left(m_p^\parallel(\mathbf{r}) - m_p^\parallel(\mathbf{s}) \right) \left(m_q^\parallel(\mathbf{r}) - m_q^\parallel(\mathbf{s}) \right)\ d^2r\ d^2s, \tag{14}$$

with, $u = a(q - p)$ indicating the dependence on the layer separation. The kernels K_{vv}^u, K_{vs}^u, and K_{ss}^u depend on δ, and represent each type of magnetic charge interaction: volume-volume interaction, volume-surface interaction, and surface-surface interactions respectively.

As it stands this representation, (11), is exact, and is the precursor to more particular representations. In this form it may be referred to as a "finite-thickness" model [23]. In typical multilayer finite-thickness models, the volume-surface interactions (K_{vs} terms) are not included [15, 32]. It is further found here that, $E_{vs}^{(pq)} \simeq \mathcal{O}(\delta^2)$, retroactively justifying their exclusion [18]. We therefore establish the asymptotic hierarchy:

$$1 \gg E_{vol}^{(pq)} \sim E_{surf}^{(pq)} \sim \delta \gg E_{vs}^{(pq)} \sim \delta^2 \tag{15}$$

In the asymptotic limit, as $\delta \to 0$, the leading order terms, $-\|m_{p,\perp}\|^2_{L^2(\mathbb{R}^2)}$, were first obtained by Gioia and James in 1997 for a thin monolayer, and all other terms are $o(1)$ [24]. Later in 2019, the $\mathcal{O}(\delta)$ terms would be rigorously obtained for the monolayer system by Knüpfer, Muratov, and Nolte [28]. The asymptotic expansion of (11) to $\mathcal{O}(\delta)$ produces the thin-film multilayer model used in [18, 5]. Finally, we may write the expansion of the stray field energy as

$$\begin{aligned} E_d(\{\mathbf{m}_i\}, \delta) = \sum_{p=1}^{N} \Bigg\{ &- ||\mathbf{m}_p^\perp||^2_{L^2} + \delta \sum_{q=1}^{N} \int_{\mathbb{R}^2} \int_{\mathbb{R}^2} \Bigg(\\ &\frac{\nabla \cdot \mathbf{m}_p^\perp(\mathbf{r}) \nabla \cdot \mathbf{m}_q^\perp(\mathbf{s})}{4\pi|\mathbf{r} - \mathbf{s}|} - \frac{(m_p^\parallel(\mathbf{r}) - m_p^\parallel(\mathbf{s}))(m_q^\parallel(\mathbf{r}) - m_q^\parallel(\mathbf{s}))}{8\pi|\mathbf{r} - \mathbf{s}|^3} \Bigg) d^2r\ d^2s \Bigg\} \\ &+ \mathcal{O}(\delta^2). \end{aligned} \tag{16}$$

3.4 Theoretical Concepts for Skyrmions

Theory of Harmonic Maps

Given the unit constraint $|\mathbf{m}| = 1$, the magnetic profile of a 2D system can be regarded as a map $\mathbf{m} : \mathbb{R}^2 \to \mathbb{S}^2$. The "Harmonic maps" are defined as minimizers of the Exchange energy,

$$E_{ex}(\mathbf{m}) = \int_{\mathbb{R}^2} |\nabla \mathbf{m}|^2 d^2r. \tag{17}$$

For a mapping between manifolds, one may define the Brouwer topological degree, q, a generalization of the winding number [40]. When we enforce $\mathbf{m} \to -\hat{\mathbf{e}}_3$ as $|\mathbf{r}| \to \infty$ then the topological degree may be expressed as

$$q(\mathbf{m}) = \frac{1}{4\pi} \int_{\mathbb{R}^2} \mathbf{m} \cdot (\partial_1 \mathbf{m} \times \partial_2 \mathbf{m})\, d^2 r, \tag{18}$$

which always takes integer values. Skyrmions in this context belong to a class of maps with degree $q = 1$. In the case of a multiple 2D systems, as is so for the multilayer ferromgantic, one defines the topological degree for each layer independently, $q(\mathbf{m}_i) = q_i$.

From the physical point of view, exchange energy is considered a dominant interaction for this problem. If other micromagnetic interactions are considered subdominant, then skyrmion solutions of (8), in the case $N = 1$, are "close" to solutions of (17), and one can attempt to generalize properties of harmonic maps to those of real skyrmions. Such studies have been carried out by Melcher in 2014 [36], and in 2017 skyrmions were shown to converge to harmonic maps in some conformal limit [20]. The general solutions of (17), restricted to $q = 1$, are called Belavin-Polyakov profiles. One such profile is

$$\mathbf{m}_\infty(\mathbf{r}) = -\frac{2\mathbf{r}}{1 + |\mathbf{r}|^2} + \frac{1 - |\mathbf{r}|^2}{1 + |\mathbf{r}|^2} \hat{\mathbf{e}}_3. \tag{19}$$

The BP-profiles exhibit 6 free parameters corresponding to dilation, translation in 2D, and SO(3) invariance [2]. These map parameters are important skyrmion properties, as they may become fixed through the minimization of other magnetic energies [7, 8].

The Restricted Class and Reduced Energy

An appropriate search space should be proposed to mathematically express and select the characteristic features of skyrmions. We therefore define the so called restricted class with desirable properties, let

$$\mathcal{A} = \left\{ \mathbf{m} \in H^1_{\text{loc}}(\mathbb{R}^2; \mathbb{S}^2) \;\middle|\; \mathbf{m} + \hat{\mathbf{e}}_3 \in H^1(\mathbb{R}^2; \mathbb{R}^3), \int_{\mathbb{R}^2} |\nabla \mathbf{m}|^2 d^2 r < 16\pi,\ q(\mathbf{m}) = 1 \right\}, \tag{20}$$

and the energy, (8) with $N = 1$, restricted to $\mathbf{m} \in \mathcal{A}$ is referred to as the "reduced energy". Bernand-Mantel et al. use the restricted class and reduced energy to flesh out the properties of skyrmion solutions [8]. This class also selects the end behavior $\mathbf{m} \to -\hat{\mathbf{e}}_3$ as $\mathbf{r} \to \infty$, removing one degree of freedom from the set of harmonic maps.

The BP-profile, (19), as it stands is not a member of the restricted class, but requires a truncation such that it becomes an $L^2(\mathbb{R}^2)$ function and may then serve as an ansatz for calculating approximate skyrmion energies [7]. This restriction is imposed such that it results in a profile with bounded anisotropy energy.

Physical Interpretation of BP Parameters

Truncated BP-profiles can be denoted $\mathbf{m}_L$ such that $\mathbf{m}_L(\mathbf{r}) = \mathbf{m}_\infty(\mathbf{r})$, for $|\mathbf{r}|^2 \leq L$, [7]. The nature of truncation divides the plane, $\mathbb{R}^2$, into characteristic regions "core" and "tail" where the majority of variation of $\mathbf{m}$ is confined to a bounded set containing the core, and outside this set the profile rapidly decays to $-\hat{\mathbf{e}}_3$. This partition localizes the phenomenon in space [8, 44], and the ansatz yields easy evaluations of (8).

Furthermore, the imposed property, $\mathbf{m} \to -\hat{\mathbf{e}}_3$, restricts the rotational freedom of these profiles to in-plane rotations only. So we may define a rotation matrix, R_θ, and write a general profile as follows,

$$\mathbf{m}(\mathbf{r}) = R_\theta \mathbf{m}_L(\mathbf{r}/\rho), \tag{21}$$

where the dilation ρ is defined as the skyrmion radius, as it marks the point for which the vector field is completely in-plane, i.e. $|\mathbf{r}| = \rho \Rightarrow \hat{\mathbf{e}}_3 \cdot \mathbf{m} = 0$. The rotational angle, θ identifies the Néel /Bloch character of the skyrmion, where $\theta = 0 \pm n\pi$ are Néel skyrmions, and $\theta = \pi/2 \pm n\pi$ are Bloch skyrmions, and those with intermediate angles are called 'Hybrids'. These are graphed for $\theta = \{\pi/2, \pi/4, 0\}$ Figure 1 (a, b, c, respectively).

4 Results and Future Work

4.1 Locus of Stable Bloch Skyrmions in Finite Thickness Monolayers

In the case of a monolayer, $N = 1$, by analyzing the stray field integral in the thin film model without asymptotically expanding in the parameter, δ, one reveals the relationship between the stray field interaction and the anisotropy strength, Q. It is shown that in the regime with small δ and small $\frac{\delta}{Q-1}$ there exists a critical $Q = Q_c(\delta)$ for which the system energy for truncated BP-profiles undergoes a bifurcation after which skyrmion solutions fail to exist. This disappearance regime is not revealed in the asymptotic model. The result contributes toward a complete description of skyrmion existence in the (Q, δ) phase space, the other boundary being the critical value of $\delta = \delta_b(Q)$ for which the skyrmion cannot be a stable compact object and bursts into magnetic domains.

For this study, begin with the model energy equation of a monolayer which includes the usual exchange and perpendicular magnetic anisotropy (PMA) and a general expression of the stray field. Let $\tilde{\mathbf{m}} : \mathbb{R}^2 \times (0, \delta) \to \mathbb{R}^3$ and $\partial_3 \mathbf{m} = 0$, that integration may be carried out in the third coordinate trivially for all local energy terms. In other words $\tilde{\mathbf{m}} = \mathbf{m}(x, y)\chi_{(0,\delta)}(z)$. Simplifying from (11), the energy is

$$E(\tilde{\mathbf{m}}) = \int_{\mathbb{R}^2} \left(|\nabla \mathbf{m}|^2 + Q|\mathbf{m}_\perp|^2 \right) d^2r + E_d\left(\tilde{\mathbf{m}}, \delta\right), \tag{22}$$

with

$$E_d\left(\tilde{\mathbf{m}}, \delta\right) = -\left\|\mathbf{m}_\perp\right\|^2_{L^2(\mathbb{R}^2)} + E_{vol}(\mathbf{m}_\perp, \mathbf{m}_\perp, \delta) + E_{surf}(m_\parallel, m_\parallel, \delta) \tag{23}$$

Supposing $\mathbf{m}$ is taken as a truncated BP-profile, (19), and a member of $\mathcal{A}$, we have a reduced energy that depends on finitely many parameters: skyrmion radius, ρ; rotation angle, θ; and truncation parameter, L:

$$E(\tilde{\mathbf{m}}) \simeq E_{\rho,\theta,L} \tag{24}$$

the minimization procedure immediately selects $E_{vol} = 0$, with the choice of minimizing rotation angles $\theta_0 = \frac{\pi}{2} \pm n\pi$, for integers, n, corresponding to Bloch skyrmions. This also solves the truncation parameter parametrically in terms of the radius $L = L_0(\rho) = (\rho\sqrt{Q-1})^{-1}$. Leaving a function of only one variable, ρ.

$$E_{\rho,\theta_0,L_0(\rho)} = 8\pi + \frac{4\pi}{L^2} + 4\pi(Q-1)\rho^2 \log\left(\frac{4L^2}{e^{2(1+\gamma)}}\right) - \delta\rho H\left(\rho/\delta\right). \tag{25}$$

Where H is a nonelementary integral coming from E_{surf}, which is rather difficult to evaluate accurately [48]. The surface charge is now the interaction which can facilitate minimizers with $\rho > 0$ which we interpret as candidate skyrmions. The character of these solutions will depend on the material parameters Q and δ.

There exists a central parameter region in the (Q, δ) plane where the energy has two or three critical points (Figure 3a), one observes a local maximum ρ_{sad}, a local minimizer ρ_{sky} denoting the skyrmion solution, and a local maximum ρ_{burst}. The final, ρ_{burst} also appears in the thin film asymptotic formulation [7], far flung of the asymptotic assumptions, yet here it plays a role in characterizing the physics at the boundary of the obtainable skyrmion solutions. Increasing δ until ρ_{burst} and ρ_{sky} annihilate one another results in an energy which has no minimizer and decreases without bound as ρ increases. This may be called the "Bursting" phase, as the calculation being done for BP-profiles suggests any BP profile will dynamically expand into a domain until it exits the restricted class, (20), by violating $\int_{\mathbb{R}^2} |\nabla \mathbf{m}|^2 d^2r < 16\pi$. Analysis of the thin film equations of [7] finds this bursting bifurcation at the following locus:

$$\delta_b = \bar{\delta}_b\sqrt{(Q_b - 1)}, \tag{26}$$

for a constant $\bar{\delta}_b = 1.97$. However, micromagnetic simulations are able to resolve skyrmion solutions far aflung of this estimate (see Figure 4). We estimate the critical parameters for this bursting by extrapolating from numerical solutions of the LLG equations to find $\bar{\delta}_b = 2.953$. It is clear, however, that more work needs to be done to resolve the bursting transition from the numerical simulations.

Meanwhile, decreasing δ until ρ_{sad} and ρ_{sky} annihilate gives a system with only the maximizer ρ_{burst}, as illustrated in Figure 3d. Thus, a BP profile as an initial condition, and subject to asymptotic assumptions, ρ may be taken smaller than ρ_{burst}, cannot minimize the energy to a radius greater than

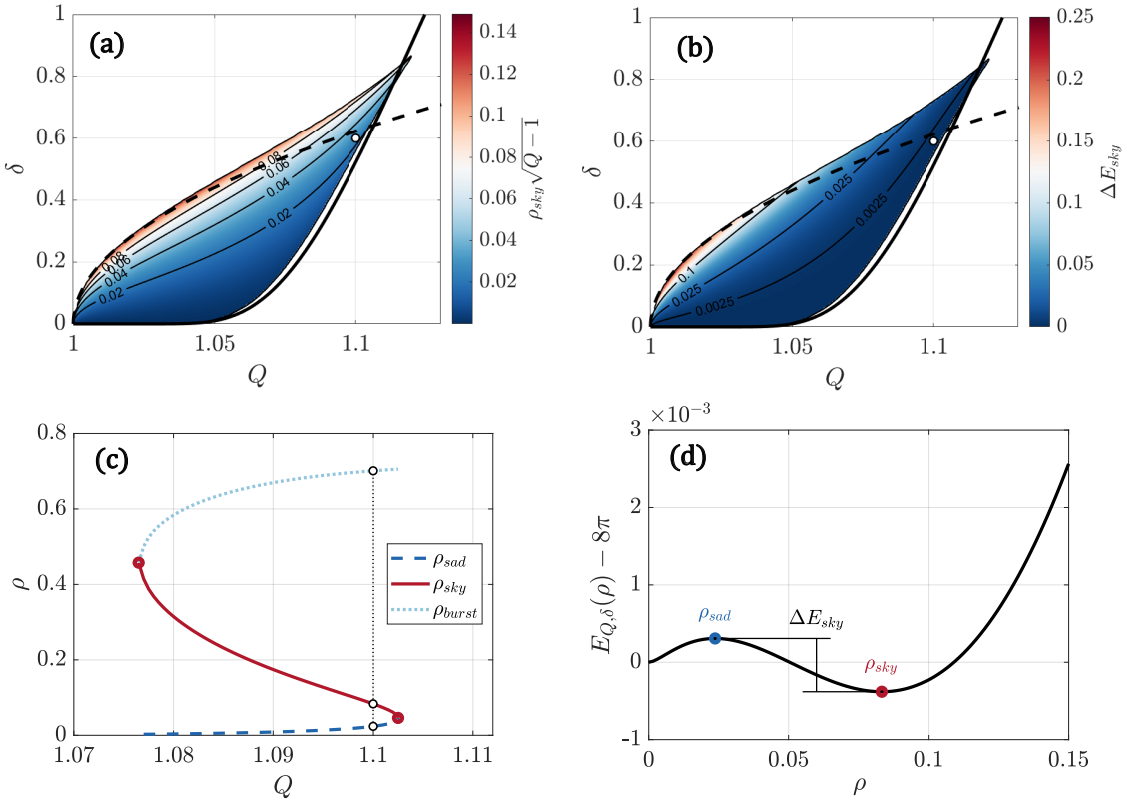

Figure 3: All skyrmion solutions for the finite-thickness model. (a) Phase diagram showing obtained skyrmion radius $\rho_{sky}\sqrt{Q-1}$ on the colormap. (b) Phase diagram showing collapse energy (27) on the colormap. (c) A locus of energy critical points for a chosen $\delta = 0.6$, and Q on the abscissa. (d) Energy landscape for parameters $Q = 1.10$ and $\delta = 0.6$ (this point in parameter space is marked with white dots on (a-b-c)). On the phase diagrams (a-b), the solid line shows the formula, (30), fitted to the collapse curve with $B = 35.18$. The dotted line shows the transition to the bursting phase predicted by the thin-film equations, (26).

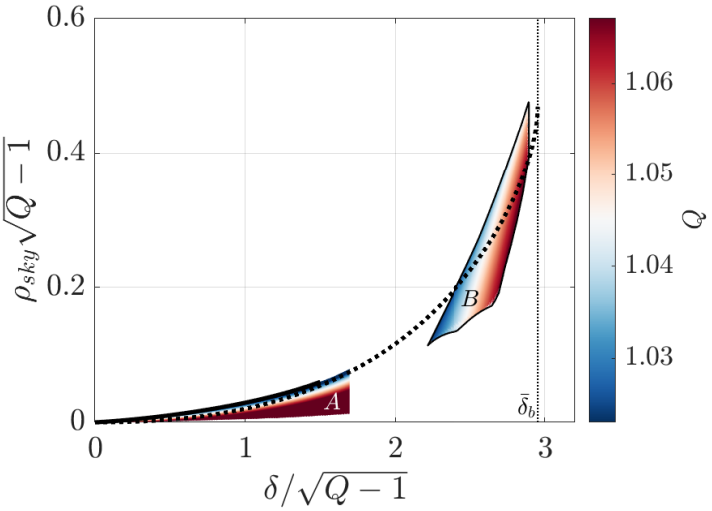

Figure 4: Simulation results compared with theoretical solutions. Dashed line: Fit between asymptotic theory and simulation results. Thin dotted line: critical value of $\bar{\delta}_b = 2.953$ obtained from fit. Region (A): skyrmion solutions resolved by the finite-thickness film theory, truncated to $\bar{\delta} \leq 1.6$. Region (B): skyrmions resolved in numerical simulation.

zero, suggesting these profiles dynamically shrink and find no stable state within the restricted class. As such we call this the "collapse" phase. In this case the collapse energy is

$$\Delta E = E(\rho_{sad}) - E(\rho_{sky}). \tag{27}$$

when the local maximizer, ρ_{sad}, does not exist, the collapse energy is just

$$\Delta E = 8\pi - E(\rho_{sky}). \tag{28}$$

The following theorem is to appear in one of our upcoming papers [4]:

Theorem 1 *The reduced energy equation calculated for BP profiles, (25), admits a minimizer over* $(0,1) \times (L_0, \infty)$ *for* δ *and* $\frac{\delta}{\sqrt{Q-1}}$ *sufficiently small and* $L_0 > 1$ *sufficiently big (all universal) if and only if for some universal constant* $B > 0$ *we have*

$$\beta = (Q-1)\left|\log \frac{BK^\star}{(Q-1)^3\delta^2}\right| < 1, \tag{29}$$

and $Q - 1$ *sufficiently small depending on* $1 - \beta$.

We remark that from this inequality we obtain a form to estimate the boundary of skyrmion existence by saturating this inequality on the positive side of the absolute value. We thereby derive the following relationship between the coordinates, (Q_c, δ_c), of the bifurcation.

$$\delta_c^2 = \frac{1}{BK^\star} \frac{\exp\left(-\frac{1}{Q_c-1}\right)}{(Q_c-1)^3}. \tag{30}$$

This critical line is shown on Figure 3.

In the numerical simulations, a skyrmion collapse corresponding to the mergers of ρ_{sky} and ρ_{sad} into a saddle node would correspond to a decreasing ρ_{sky}. In Figure 4, this is the bottom boundary of the solution loci. The future direction of this simulation work will involve unifying the collapse curve of the theoretical and numerical simulations. It may well be the case that the problem is so numerically stiff that little solution overlap between the theory and numerics will occur in practice. If so, one can still proceed to resolve identical qualitative trends between both of these families. We are at work testing this problem on a few softwares, such as the mumax3 software [49] which was used to obtain the present results, as well as the Excalibur software [45].

Future studies of systems of this type may reintroduce the more commonly studied DMI, $\kappa > 0$. The model equation here has $\kappa = 0$, and suggests that the contribution of very small κ could lead to the formation of a second minimizer $\rho_{sky-2} < \rho_{sad}$, however it will also compete with the volume charge interaction $E_{vol} > 0$.

4.2 Skyrmions in Stray-Field Coupled Multi-Layers

We treat the multilayer ferromagnetic system with no DMI, where the layers interact with each other through the stray field only. We therefore take $\kappa_i = 0$ and $\sigma = 0$. The energy equation for a thin N-layer system is (8), where the stray field is given by the asymptotic formula (16).

We can search for minimizers in the restricted class of skyrmion profiles. This can be shown by ansatz based minimization of the thin film multilayer energy among the class of Belavin-Polyakov profiles. We treat the N layer case to show the existence of same-size skyrmion columns in a system governed by the exchange, anisotropy, and stray field interactions alone. We will also examine the particular case of 2 layers, which allows a more granular look at the energy landscape and gives insight into possible dynamics when skyrmions in different layers are separated by a nonzero distance. This reveals a saddle point in the skyrmion separation parameter, above a critical value the interaction is repulsive rather than attractive.

An additional displacement parameter for the BP-profiles is introduced, l_{ij}, representing the distance between the cores of the skyrmions in layer i and j. This form of the energy also admits further

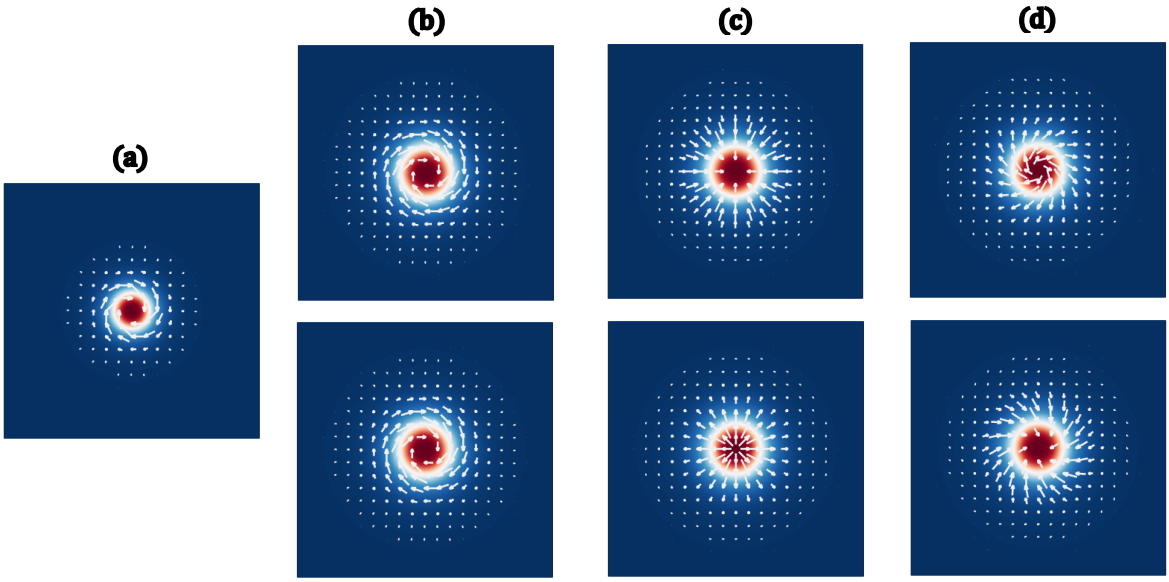

Figure 5: Comparison of several species of bilayer skyrmions represented by plots of BP-profiles with all layers of thickness $\bar{\delta}$ and radii obtained from theorem 2. (a) Monolayer Bloch skyrmion. (b-c-d) Bilayer skyrmions. (b-c-d) Result in skyrmions of larger radii than would be obtained by a monolayer of depth $\bar{\delta}$. A bilayer system with concentric skyrmions in each layer admits precession of the in-plane angle, such that the radial components of the magnetization in each layer will be opposite. Thus one may have (b) concentric Bloch skyrmions, (c) opposite Néel skyrmions, (d) hybrid skyrmions having opposite radial components.

renormalization, with $\bar{\delta} = \delta/\sqrt{Q-1}$, and the replacement $\rho_i\sqrt{Q-1} \to \rho_i$. So, the reduced energy becomes:

$$\begin{aligned} E = &\sum_{i=1}^{N}\left[8\pi + \frac{4\pi}{L_i^2} + 4\pi\rho_i^2\log\left(\frac{4L_i^2}{e^{2(1+\gamma)}}\right) + \bar{\delta}\frac{\pi^3}{8}\rho_i(3\cos^2\theta_i - 1)\right] \\ &+ \sum_{i=1}^{N}\sum_{j<i}\bar{\delta}\frac{\pi^3}{4}\sqrt{\rho_i\rho_j}\left[3\cos\theta_i\cos\theta_j F_v\left(\sqrt{\frac{\rho_j}{\rho_i}}, \frac{l_{ij}}{\sqrt{\rho_i\rho_j}}\right) - F_s\left(\sqrt{\frac{\rho_j}{\rho_i}}, \frac{l_{ij}}{\sqrt{\rho_i\rho_j}}\right)\right]. \end{aligned} \tag{31}$$

where the functions F_v and F_s are nonelementary integrals derived from the asymptotic forms of $E_{vol}^{(ij)}$ and $E_{surf}^{(ij)}$.

The following theorem gives the existence and the form of the solutions, it is proved in my thesis and also to appear in one of our papers [5, 18].

Theorem 2 *Let $i, N \in \mathbb{N}$ with $1 \le i \le N$ and $\rho_i \in \left(0, \frac{2}{e^{2+\gamma}}\right)$. Then the minimizers of the energy E defined in (31) satisfy*

1. $\rho_i = \rho = -\frac{B}{2W(-\frac{B\sqrt{A}}{2})}$, *where* $A = \frac{e^{2+2\gamma}}{4}$, $B = \frac{N\bar{\delta}\pi^2}{64}$ *and W is a Lambert W function;*
2. *for $1 \le j < i \le N$ it holds $l_{ij} = 0$;*
3. $L_i = \rho^{-1}$;
4. $\sum_{i=1}^{N}\cos\theta_i = 0$.

This gives the existence of skyrmion solutions with the skyrmions in each layer forming a same size $\forall i, \rho = \rho_i$, where ρ depends only on the universal parameter $N\bar{\delta}$. They appear in a concentric column, ($l_{ij} = 0$). Most interestingly, the solution for the angles gives a very lax constraint $\sum\cos\theta_i = 0$. In this state the minimizing θ_i have $N-1$ degrees of freedom, and may precess freely between Néel,

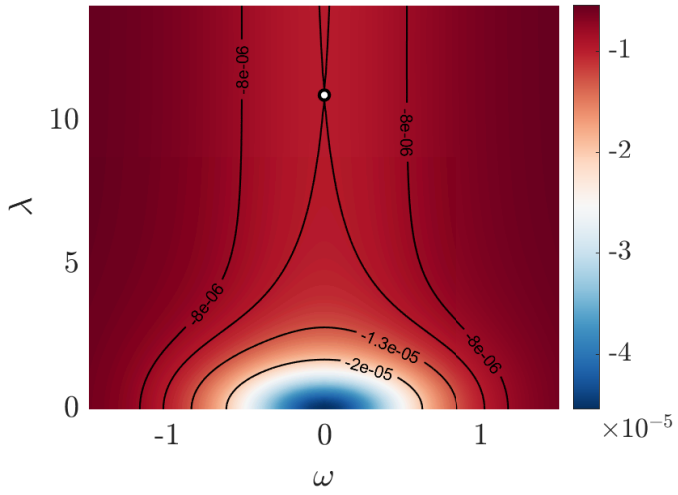

Figure 6: Energy after minimizing in ρ. Parameter values are $\bar{\kappa} = 0$, $\bar{\sigma} = 0$, $\bar{\delta} = 0.07$. The system favors a bound state where the skyrmions are concentric and perfectly symmetric $(\omega, \lambda) = (0, 0)$. Alternatively, note the presence of a saddle at $(\omega, \lambda) = (0, 10.9)$ beyond which, the skyrmion interaction is repulsive.

Bloch, and Hybrid skyrmions so long as the constraint is obeyed. Examples of skyrmion solutions in this system are shown in Figure 5.

More restricted analysis of the case $N = 2$ can reveal more granular dynamics at work in the energy landscape. Let $\omega = \frac{1}{2}\log\left(\frac{\rho_2}{\rho_1}\right)$, and $\lambda = \frac{l_{12}}{\sqrt{\rho_1\rho_2}}$. When (31) is parametrically minimized in each parameter except ω, λ, we see same size skyrmions are clearly favored in all cases, (Figure 6). Additionally for λ larger than $\lambda_s = 10.9$, the energy crosses a saddle point, beyond which the skyrmions would experience a repulsive interaction, and run away to infinity. The value of λ_s is universal in this system and does not depend on $\bar{\delta}$. Finally, allowing λ to vary, as we have, changes the volume charge energy, which further constrains the rotation angles θ_i. They only exhibit the freedom given by theorem 2 when $\lambda = 0$, and otherwise are constrained to identical Bloch skyrmions $\theta_i = \frac{\pi}{2} \pm n\pi$, as in Figure 5.b.

4.3 Néel Skyrimons in Excahnge Coupled Bilayers

The second mechanism that couples multilayer systems is the exchange coupling, characterized by the constant σ in (8). The exchange coupling is a local interaction, and each layer only interacts with its neighboring layers. This is to be contrasted with the stray field coupling studied in the previous section, which is nonlocal and facilitates the simultaneous interaction of every layer in the system. The exchange coupling could also be ferromagnetic or antiferromagnetic depending on the sign of σ [29, 41]. Here, analyzing the antiferromangetic order would involve changing the ansatz in one of the layers, say layer-j, such that $\mathbf{m}_j \to +\hat{\mathbf{e}}_3$ as $\mathbf{r} \to \infty$, amounting to a reversal of the out-of-plane component, $m_{j,\parallel} \to -m_{j,\parallel}$.

We proceed with the same energy equation, (8), and suppress the stray field coupling by setting $\delta = 0$, keeping only the leading order stray field interaction. Thus,

$$E_d(\{\mathbf{m}_i\}, 0) = -\sum_{i=1}^{N} \|\mathbf{m}_{i,\perp}\|^2_{L^2(\mathbb{R}^2)} \,. \tag{32}$$

This leaves the DMI as the skyrmion enabling interaction, so $\kappa_i > 0$. For simplicity's sake we restrict the following calculation to that of a bilayer system. We will use the rescalings

$$\bar{\kappa}_i = \kappa_i/\sqrt{Q-1}\,, \quad \bar{\sigma} = \sigma/\sqrt{Q-1}\,, \quad \rho\sqrt{Q-1} \to \rho \tag{33}$$

The form of the exchange coupling energy makes for difficult calculations on BP-profiles. It is well defined for truncations $L < \infty$, but to leading order in $L \to \infty$ it is a divergent integral except when

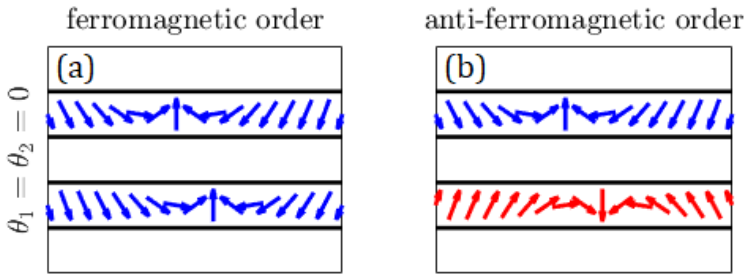

Figure 7: Illustration of the two configurations for the exchange coupled bilayer problem with Néel skyrmion pairs. The pictured skyrmions have in-plane angles which would be selected by the following DMI strengths: in the top layer $\bar{\kappa}_1 > 0$, (a) has $\bar{\kappa}_2 = \bar{\kappa}_1$, leading to two counterclockwise Néel skyrmions. (b) has $\bar{\kappa}_2 = -\bar{\kappa}_1$ resulting in one counterclockwise and one clockwise Néel skyrmion.

the skyrmions in neighboring layers have the same size, $\rho_1 = \rho_2 = \rho$ and the same rotation angle, $\theta_1 = \theta_2$. Since it is always positive in its definition, we can provisionally interpret this as a large energy penalty that helps select the minimizing profiles. Let the separation parameter be $\lambda = \frac{l_{12}}{\sqrt{\rho_1 \rho_2}}$, we find in both the ferromangetic and antiferromangnetic case:

$$E_{ec}(\mathbf{m}_1, \mathbf{m}_2) = 16\pi|\bar{\sigma}|\rho^2 \left(\frac{\lambda \sinh^{-1}(\lambda/2)}{\sqrt{\lambda^2 + 4}} \right). \tag{34}$$

It is found in carrying out the energy minimization that certain configurations lead to a cancellation of the total DMI energy of the system. For the ferromagnetic order, under the present assumptions, opposite sign DMI will cancel out and leave an energy which is strictly increasing in ρ, and therefore no minimizer $\rho > 0$ can be found. We say there are no skyrmion solutions. The same is true for an antiferromagnetic order where the two layers have same-sign DMI, $\bar{\kappa}_1 = \bar{\kappa}_2$.

In the other two cases, those with a ferromagnetic order and same-sign DMI and antiferromagnetic orders with opposite sign DMI, One finds Néel skyrmion solutions, as in Figure 7. Indeed, the minimizing separation is $\lambda = 0$ so they will be concentric and of the same size. A curious consequence is that one finds the skyrmion size ρ does not depend explicitly on $\bar{\sigma}$. So the exchange coupling does not play a role in determining the skyrmion size, but only penalizes deviations from $\lambda = 0$.

Having suppressed the stray field coupling, the reintroduction of a perturbative effect, $0 < \bar{\delta} \ll \bar{\sigma} \sim \bar{\kappa}$, can add new features to the energy landscape without drastically increasing the complexity of the system. Preliminary research in this direction shows the existence of new metastable states, minimizers with $\lambda > 0$ giving off-center skyrmion pairings. More work can be done here to characterize the relationship between each of the material parameters.

The numerics of this bilayer system with $\bar{\kappa} \neq 0$, and $\bar{\sigma} \neq 0$ are far better posed than that done for the finite thickness model in section 4.1. This type of bilayer problem has been treated in great detail by Koshibae and Nagaosa [29]. But they used a discrete square lattice instead of the continuous models we employ, only studying it numerically, and they also suppressed the nonlocal stray field in their study. Their success gives hope for this experiment; we intend to proceed in a similar direction with a dynamical study of bilayer skyrmions. The mumax3 software we employed should suffice to this end without the problems we encountered in section 4.1 [49].

References

[1] V. Baltz, A. Manchon, M. Tsoi, T. Moriyama, T. Ono, and Y. Tserkovnyak, *Antiferromagnetic spintronics*, Reviews of Modern Physics, 90 (2018).

[2] A. A. Belavin and A. M. Polyakov, *Metastable states of two-dimensional isotropic ferromagnets*, Journal of Experimental and Theoretical Physics Letters, (1975), pp. 245–247.

[3] A. Bernand-Mantel, L. Camosi, A. Wartelle, N. Rougemaille, M. Darques, and L. Ranno, *The skyrmion-bubble transition in a ferromagnetic thin film*, SciPost Physics, 4 (2018), p. 27.

[4] A. Bernand-Mantel, N. J. Dubicki, C. B. Muratov, and T. M. Simon, *Stray field enabled skyrmions in ferromagnetic films of finite thickness*, 2025. Manuscript in Preparation.

[5] A. Bernand-Mantel, N. J. Dubicki, C. B. Muratov, and V. V. Slastikov, *Bloch skyrmions in stray field coupled magnetic multilayers*, 2025. Manuscript in Preparation.

[6] A. Bernand-Mantel, A. Fondet, S. Barnova, T. M. Simon, and C. B. Muratov, *Theory of magnetic field stabilized compact skyrmions in thin-film ferromagnets*, Physical Review B, 108 (2023), p. L161405.

[7] A. Bernand-Mantel, C. B. Muratov, and T. M. Simon, *Unraveling the role of dipolar versus dzyaloshinskii-moriya interaction in stabilizing compact magnetic skyrmions*, Physical Review B, (2020), p. 045416.

[8] ——, *A quantitative description of skyrmions in ultrathin ferromagnetic films and rigidity of degree ±1 harmonic maps from $r2$ to $s2$*, Archive for Rational Mechanics and Analysis, (2021), pp. 219–299.

[9] A. Bernand-Mantel, C. B. Muratov, and V. V. Slastikov, *A micromagnetic theory of skyrmion lifetime in ultrathin ferromagnetic films*, Proceedings of the National Academy of Sciences of the United States of America, 119 (2022), p. 29.

[10] P. F. Bessarab, G. P. Müller, I. S. Lobanov, F. N. Rybakov, N. S. Kiselev, H. Jónsson, V. M. Uzdin, S. Blügel, L. Bergqvis, and A. Delin, *Lifetime of racetrack skyrmion*, Scientific Reports, 8 (2018), p. 3433.

[11] A. Bogdanov, M. Kudinov, and D. Yablonskii, *Theory of magnetic vortices in easy-axis ferromagnets*, Soviet Physics Solid State, 31 (1989), pp. 1707–1710.

[12] A. N. Bogdanov and D. A. Yablonskii, *Thermodynamically stable "vortices" in magnetically ordered crystals. the mixed state of magnets*, Soviet Journal of Experimental and Theoretical Physics, 95 (1989), pp. 178–182.

[13] O. Boulle, J. Vogel, H. Yang, S. Pizzini, D. D. S. Chaves, A. Locatelli, T. O. Menteş, A. Sala, L. D. Buda-Prejbeanu, O. Klein, M. Belmeguenai, Y. Roussigné, A. Stashkevich, S. M. Chérif, L. Aballe, M. Foerster, M. Chshiev, S. Auffret, I. M. Miron, and G. Gaudin, *Room-temperature chiral magnetic skyrmions in ultrathin magnetic nanostructures*, Nature Nanotechnology, 11 (2016), pp. 449–454.

[14] W. F. Brown, *Micromagnetics*, Interscience Tracts of Physics and Astronomy, Interscience Publishers (Wiley and Sons), New York, NY, USA, 1963.

[15] F. Büttner, B. Krüger, S. Eisebitt, and M. Kläui, *Accurate calculation of the transverse anisotropy of a magnetic domain wall in perpendicularly magnetized multilayers*, Physical Review B, 92 (2015).

[16] F. Büttner, I. Lemesh, and G. S. Beach, *Theory of isolated magnetic skyrmions: From fundamentals to room temperature applications*, Scientific Reports, 8 (2018).

[17] H. T. Diep, *Phase transition in frustrated magnetic thin film-physics at phase boundaries*, Entropy, 21 (2019).

[18] N. J. Dubicki, *A Micromagnetic Study of Skyrmions in Thin-Film Multilayered Ferromagnetic Materials*, PhD thesis, New Jersey Institute of Technology, Newark, New Jersey, USA, 2024.

[19] I. Dzyaloshinskii, *A thermodynamic theory of "weak" ferromagnetism of antiferromagnetics*, Journal of Physics and Chemistry of Solids, 4 (1958), pp. 241–255.

[20] L. Döring and C. Melcher, *Compactness results for static and dynamic chiral skyrmions near the conformal limit*, Calculus of Variations and Partial Differential Equations, 56 (2017).

[21] A. Fert, V. Cros, and J. Sampaio, *Skyrmions on the track*, Nature Nanotechnology, 8 (2013), pp. 152–156.

[22] G. D. Fratta, C. B. Muratov, F. N. Rybakov, and V. V. Slastikov, *Variational principles of micromagnetics revisited*, Society of Industrial and Applied Mathematics Journal on Mathematical Analysis, 52 (2020), pp. 3580–3599.

[23] C. J. García-Cervera, *Magnetic domains and magnetic domain walls*, PhD thesis, Courant Institute of Mathematical Sciences, New York University, New York, NY, USA, 1999.

[24] G. Gioia and R. D. James, *Micromagnetics of very thin films*, Proceedings of the Royal Society of London. Series A: Mathematical, Physical and Engineering Sciences, 453 (1997), pp. 213–223.

[25] J. Hagemeister, N. Romming, K. von Bergmann, E. Y. Vedmedenko, and R. Wiesendanger, *Stability of single skyrmionic bits*, Nature Communications, 6 (2015), p. 8455.

[26] A. Hubert and R. Schäfer, *Magnetic Domains: The Analysis of Magnetic Micro structures*, Springer, Berlin, Germany, 1998.

[27] T. Jungwirth, X. Marti, P. Wadley, and J. Wunderlich, *Antiferromagnetic spintronics*, Nature Nanotechnology, 11 (2016), pp. 231–241.

[28] H. Knüpfer, C. B. Muratov, and F. Nolte, *Magnetic domains in thin ferromagnetic films with strong perpendicular anisotropy*, Archive for Rational Mechanics and Analysis, 232 (2019), pp. 727–761.

[29] W. Koshibae and N. Nagaosa, *Theory of skyrmions in bilayer systems*, Scientific Reports, 7 (2017), p. 42645.

[30] L. D. Landau and E. M. Lifshitz, *On the theory of the dispersion of magnetic permeability in ferromagnetic bodies*, Physikalische Zeitschrift der Sowjetunion, 8 (1935), pp. 153–169.

[31] ——, *Electrodynamics of Continuous Media*, Pergamon Press Ltd., Oxford, UK, 1960.

[32] I. Lemesh, F. Büttner, and G. S. Beach, *Accurate model of the stripe domain phase of perpendicularly magnetized multilayers*, Physical Review B, 95 (2017).

[33] I. S. Lobanov, H. Jónsson, and V. M. Uzdin, *Mechanism and activation energy of magnetic skyrmion annihilation obtained from minimum energy path calculations*, Physical Review B, 94 (2016), p. 174418.

[34] C. T. Ma, X. Li, and S. J. Poon, *Micromagnetic simulation of ferrimagnetic tbfeco films with exchange coupled nanophases*, Journal of Magnetism and Magnetic Materials, 417 (2016), pp. 197–202.

[35] J. McCord, *Progress in magnetic domain observation by advanced magneto-optical microscopy*, Journal of Physics D: Applied Physics, 48 (2015), p. 333001.

[36] C. Melcher, *Chiral skyrmions in the plane*, Proceedings of the Royal Society A: Mathematical, Physical and Engineering Sciences, 470 (2014).

[37] T. Moriya, *Anisotropic superexchange interaction and weak ferromagnetism*, Physical Review, 120 (1960), pp. 91–98.

[38] S. Mühlbauer, B. Binz, F. Jonietz, C. Pfleiderer, A. Rosch, A. Neubauer, R. Georgii, and P. Böni, *Skyrmion lattice in a chiral magnet*, Science, 323 (2009), p. 915.

[39] F. Nolte, *Optimal scaling laws for domain patterns in thin ferromagnetic films with strong perpendicular anisotropy*, PhD thesis, Heidelberg University, Heidelberg, Germany, 2017.

[40] S. Novikov and A. Fomenko, *Basic Elements of Differential Geometry and Topology*, Springer Nature B.V., Berlin, Germany, 2010.

[41] S. Panigrahy, S. Mallick, J. a. Sampaio, and S. Rohart, *Skyrmion inertia in synthetic antiferromagnets*, Physical Review B, 106 (2022), p. 144405.

[42] M. Potkina, I. Lobanov, H. Jonsson, and V. Uzdin, *Lifetime of skyrmions in discrete systems with infinitesimal lattice constant*, Journal of Magnetism and Magnetic Materials, 549 (2022), p. 168974.

[43] N. Romming, C. Hanneken, M. Menzel, J. E. Bickel, B. Wolter, K. von Bergmann, A. Kubetzka, and R. Wiesendanger, *Writing and deleting single magnetic skyrmions*, Science, 341 (2013), pp. 636–639.

[44] M. Rupflin, *Sharp quantitative rigidity results for maps from s^2 to s^2 of general degree*, 2023.

[45] F. N. Rybakov and E. Babaev, *Excalibur software*.

[46] M. Schott, A. Bernand-Mantel, L. Ranno, S. Pizzini, J. Vogel, H. Béa, C. Baraduc, S. Auffret, G. Gaudin, and D. Givord, *The skyrmion switch: Turning magnetic skyrmion bubbles on and off with an electric field*, Nano Letters, 17 (2017), pp. 3006–3012. PMID: 28437086.

[47] Y. Tokura and N. Kanazawa, *Magnetic skyrmion materials*, Chemical Reviews, 121 (2021), pp. 2857–2897.

[48] L. N. Trefethen, *Exactness of quadrature formulas*, SIAM Review, 64 (2021), pp. 132–150.

[49] A. Vansteenkiste, J. Leliaert, M. Dvornik, M. Helsen, F. Garcia-Sanchez, and B. Van Waeyenberge, *The design and verification of mumax3*, American Institute of Physics Advances, 4 (2014), p. 107133.

[50] S. Woo, K. Litzius, B. Krüger, M. Y. Im, L. Caretta, K. Richter, M. Mann, A. Krone, R. M. Reeve, M. Weigand, P. Agrawal, I. Lemesh, M. A. Mawass, P. Fischer, M. Kläui, and G. S. Beach, *Observation of room-temperature magnetic skyrmions and their current-driven dynamics in ultrathin metallic ferromagnets*, Nature Materials, 15 (2016), pp. 501–506.

[51] J. Zázvorka, F. Jakobs, D. Heinze, N. Keil, S. Kromin, S. Jaiswal, K. Litzius, G. Jakob, P. Virnau, D. Pinna, K. Everschor-Sitte, L. Rózsa, A. Donges, U. Nowak, and M. Kläui, *Thermal skyrmion diffusion used in a reshuffler device*, Nature Nanotechnology, 14 (2019), pp. 658–661.